Generation of sub-diffraction-limited pure longitudinal magnetization by the inverse Faraday effect by tightly focusing an azimuthally polarized vortex beam

Yunshan Jiang,[1,2] Xiangping Li,[1] and Min Gu[1,]*

[1]Centre for Micro-Photonics, Faculty of Engineering and Industrial Sciences, Swinburne University of Technology, Hawthorn VIC 3122, Australia

[2]Department of Optical Engineering, Zhejiang University, Hangzhou 310027, China
*Corresponding author: mgu@swin.edu.au

In this Letter we report on the generation of sub-diffraction-limited pure longitudinal magnetization in optomagnetic materials. The interaction between polarization singularities of cylindrically polarized beams and optical vortices in the tight focus of a high numerical-aperture objective as well as the induced magnetic fields through the inverse Faraday effect are investigated. A pure longitudinal magnetization distribution throughout the entire focal plane, which has a 15% reduction in the lateral full width at half-maximum, is achieved by tightly focusing an azimuthally polarized vortex beam. © 2013 Optical Society of America

OCIS codes: (210.3820) Magneto-optical materials; (260.1960) Diffraction theory; (260.5430) Polarization; (210.3810) Magneto-optic systems.
http://dx.doi.org/10.1364/OL.38.002957

The discovery of the giant magnetoresistance [1] has facilitated longitudinal magnetization (normal to the surface of a recording medium) in recording with a granular size of sub-hundred nanometers and thus accelerated the development of high capacity magnetic storage devices. Recently, the inverse Faraday effect (IFE), conceived in the 1960s [2] for all-optical magnetic recording (AOMR), has emerged as a key component for the next generation storage technology of an ultra-high areal density [3–5]. In AOMR, the magnetization reversal induced by focusing a circularly polarized beam with an objective [3,4] has been demonstrated to be an essential method for the longitudinal magnetization recording. However, the degree of the longitudinal magnetization in this case can be degraded due to the depolarization effect by an objective of high numerical aperture (NA) which is a necessity for sub-wavelength AOMR.

As is well known, the control of the phase, amplitude, and polarization distributions of a laser beam at the back aperture of a high NA objective can lead to enriched electric field components within its focus [6,7] and thus shape both the spatial distribution and the orientation of the light-induced magnetization by the IFE. As such, focusing a radially polarized beam has resulted in vortex-like transverse magnetization [8], although this outcome is not necessarily useful for high density AOMR. On the other hand, the binary phase [9,10] and amplitude modulation [11] of an incident beam has been used to improve the spatial resolution at the cost of the accompanying detrimental transverse magnetization. Thus, generating pure longitudinal magnetization within a sub-diffraction-limited region by the IFE has remained a challenge toward sub-wavelength AOMR. In this Letter, we demonstrate that sub-wavelength AOMR with pure longitudinal magnetization throughout the entire focal plane of a high NA objective is possible when an azimuthally polarized beam is superposed with an optical vortex.

As has been demonstrated [12,13], optical vortex beams focused by a high NA objective can result in a dramatic change in the distribution of the electric fields within the focus. Since the azimuthally polarized beam, or in general a cylindrically polarized beam, can be seen as the superposition of circularly polarized beams of an opposite circular direction, let us first consider the focusing property of the left/right-handed circularly (LHC/RHC) polarized beam with vortices described by topological charge m. The incident beam can be expressed as $[\mathbf{E}_x, \mathbf{E}_y, \mathbf{E}_z] = [1, \pm i, 0] \exp(im\varphi_s)$ (positive for LHC and negative for RHC). Based on the vectorial Debye diffraction theory [6], at point (ρ_s, φ_s, z_s) within the focal vicinity of an aplanatic lens, the focal electric fields of LHC and RHC polarized vortex beams can be expressed, in cylindrical coordinates, as

$$\mathbf{E}^{L/\mathrm{RHC}}(\rho_s, \varphi_s, z_s)$$

$$= \begin{bmatrix} \mathbf{E}_\rho \\ \mathbf{E}_\varphi \\ \mathbf{E}_z \end{bmatrix} = i^m C e^{i(m\pm 1)\varphi_s} \begin{bmatrix} i[R_1(m\pm 1) \mp A_1(m\pm 1)] \\ [R_2(m\pm 1) \mp A_2(m\pm 1)] \\ 2R_3(m\pm 1) \end{bmatrix}, \quad (1)$$

$$\begin{cases} R_1(n) = \int_0^\alpha P_0(\theta)\sin\theta\cos\theta[J_{n+1}(k\rho_s\sin\theta) - J_{n-1}(k\rho_s\sin\theta)] \\ \qquad * \exp(ikz_s\cos\theta)\mathrm{d}\theta, \\ R_2(n) = \int_0^\alpha P_0(\theta)\sin\theta\cos\theta[J_{n+1}(k\rho_s\sin\theta) + J_{n-1}(k\rho_s\sin\theta)] \\ \qquad * \exp(ikz_s\cos\theta)\mathrm{d}\theta, \\ R_3(n) = \int_0^\alpha P_0(\theta)\sin^2\theta J_n(k\rho_s\sin\theta)\exp(ikz_s\cos\theta)\mathrm{d}\theta, \\ A_1(n) = \int_0^\alpha P_0(\theta)\sin\theta[J_{n+1}(k\rho_s\sin\theta) + J_{n-1}(k\rho_s\sin\theta)] \\ \qquad * \exp(ikz_s\cos\theta)\mathrm{d}\theta, \\ A_2(n) = \int_0^\alpha P_0(\theta)\sin\theta[J_{n+1}(k\rho_s\sin\theta) - J_{n-1}(k\rho_s\sin\theta)] \\ \qquad * \exp(ikz_s\cos\theta)\mathrm{d}\theta, \end{cases}$$

$$(2)$$

where C is a constant, α is the convergence semi-angle of the lens, $P_0(\theta) = l_0(\theta)\cos^{1/2}(\theta)$ represents the pupil

function, and for the uniform illumination $l_0(\theta) = 1$. J_n is the nth Bessel function of the first kind. $k = 2\pi/\lambda = nk_0$ is the wave factor in image space. It should be noted that terms A_1 and R_2 are unnecessarily ignored in the previous literature [12], which could lead to the consequent light-induced magnetization with incorrect characteristics.

Based on the free-energy function [14], the magnetization field induced by the IFE through focusing a circularly polarized vortex beam in the isotropic magnetically ordered material can be expressed as

$$\mathbf{M} = i\gamma \mathbf{E} \times \mathbf{E}^*, \tag{3}$$

where $\mathbf{E}$ is the electric field, $\mathbf{E}^*$ represents its conjugate, and γ is the coupling efficiency proportional to the magneto-optical susceptibility χ of the material. By substituting Eqs. (1) and (2) into Eq. (3), the induced magnetization field by the tightly focused LHC polarized vortex beam can be given by

$$\mathbf{M}^{\mathrm{LHC}}(\rho_s, \varphi_s, z_s) = \begin{bmatrix} \mathbf{M}_\rho \\ \mathbf{M}_\varphi \\ \mathbf{M}_z \end{bmatrix} = C' \begin{bmatrix} -2\,\mathrm{Im}[(R_2(m+1) - A_2(m+1)) * R_3^*(m+1)] \\ 2\,\mathrm{Re}[(R_1(m+1) - A_1(m+1)) * R_3^*(m+1)] \\ -\mathrm{Re}[(R_1(m+1) - A_1(m+1)) * (R_2(m+1) - A_2(m+1))^*] \end{bmatrix}, \tag{4}$$

where $C' = 2\gamma C^2$ is a constant. The induced magnetization field in the focal plane of a LHC polarized beam with a topological charge of 0, –1, and +1, respectively, are shown in Fig. 1. The total magnetization field is calculated as $\mathbf{M} = (\mathbf{M}_\rho^2 + \mathbf{M}_\varphi^2 + \mathbf{M}_z^2)^{1/2}$ and is normalized to unity by the maximum magnetization induced by the LHC polarized beam with $m = 0$. Since the nonzero radial magnetization components only exist in the out-of-focus area [15], it is not presented here. In the
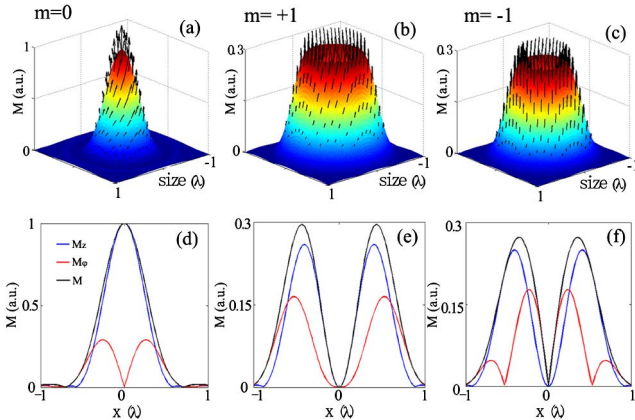

Fig. 1. Distribution of the light-induced magnetization in the focal plane of tightly focused LHC polarized beams with a topological charge of (a) 0, (b) +1, and (c) –1. Arrows indicate the orientation of the magnetization. (d)–(f) Cross-section plots of normalized longitudinal (M_z, blue curves), azimuthal (M_φ, red curves), and total magnetization (M, black curves). The radial magnetization field is null in the focal plane and not shown.

calculation, NA = 0.95 and the refractive index of 1 are used. The results for the RHC polarized vortex beam are not presented here, since they are analogous to those of the LHC polarized vortex beam.

The interaction between optical vortices and the circular polarization field can dramatically change the spatial distribution of the resultant magnetization field. A Gaussian-shape-like longitudinal magnetization distribution is dominant in the focal plane of the LHC polarized beam without vortices, accompanied by a portion (23%) of doughnut-shaped transverse magnetization [Fig. 1(a)]. When an optical vortex is present, the generated magnetization distribution has a doughnut shape with an increased lateral full width at half-maximum (FWHM), and the ratio of the transverse component varies as the helicity of vortex changes, ranging from 15.96% ($m = -1$) to 27.11% ($m = +1$). Though the presence of optical vortices may suppress the transverse magnetic component, the resultant doughnut-shaped magnetization spot does not favor high density AOMR.

The mutual effect between polarization singularities of cylindrically polarized beams and optical vortices cannot only change the spatial distribution but also the orientation of the dominant magnetization field. As one kind of polarization singularities, a radially polarized beam with a topological charge of m can be expressed as the superposition of two circularly polarized vortex beams, $\mathbf{E}^{\mathrm{Rad}} = 1/2[\mathbf{E}^{\mathrm{LHC}}(m-1) + \mathbf{E}^{\mathrm{RHC}}(m+1)]$. Based on the mathematically corrected expression for focused circularly polarized vortex beams and Eq. (3), the light-induced magnetization for radially polarized vortex beams can be given as

$$\mathbf{M}^{\mathrm{Rad}}(\rho_s, \varphi_s, z_s) = \begin{bmatrix} \mathbf{M}_\rho \\ \mathbf{M}_\varphi \\ \mathbf{M}_z \end{bmatrix} = C' \begin{bmatrix} -2\,\mathrm{Im}[R_2(m) * R_3^*(m)] \\ 2\,\mathrm{Re}[R_1(m) * R_3^*(m)] \\ -\mathrm{Re}[R_1(m) * R_2^*(m)] \end{bmatrix}. \tag{5}$$

When $m = 0$, the light-induced magnetization is a pure transverse magnetic vortex [8]. Interestingly, for a radially polarized beam with a topological charge $m = 1$, a flap-top magnetization with a dominant longitudinal component in the focal vicinity is generated in Fig. 2.

To gain insight on the interaction between polarization singularities and optical vortices, let us first consider the case under the low NA condition. For each ring ($d\theta$) of the exit pupil, its contribution to the electric field components on the focus point can be expressed as
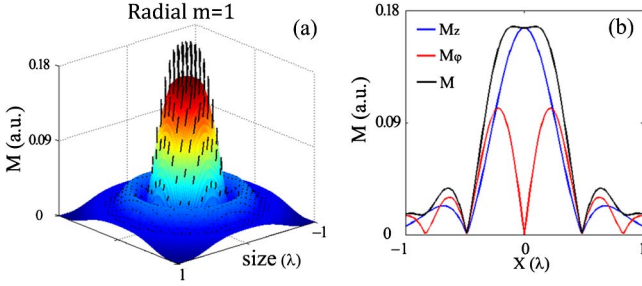
Fig. 2.   (a) Spatial distribution and (b) cross-section plot of light-induced magnetization by the IFE through tightly focusing radially polarized beams with a topologic charge of $m = 1$.

$$E^{\text{Rad}}(0,0,0) = \begin{bmatrix} E_x \\ E_y \\ E_z \end{bmatrix} = \begin{bmatrix} \int_0^{2\pi} \cos\varphi e^{\pm i\varphi} d\varphi \\ \int_0^{2\pi} \sin\varphi e^{\pm i\varphi} d\varphi \\ 0 \end{bmatrix} = \pi \begin{bmatrix} 1 \\ \pm i \\ 0 \end{bmatrix}. \tag{6}$$

From Eq. (6), it can be seen that circular polarization is generated on the focus voxel, owing to the mutual effect of the polarization singularity of the cylindrically polarized beam and the optical vortex. The orientation of the longitudinal magnetization is determined by the helicity of the spiral phase. However, in the case of tight focusing by a high NA objective (NA = 0.95), the enhanced longitudinal electric field components result in a large portion (30%) of the transverse magnetic field in the off-axis area.

On the other hand, the interaction between the polarization singularity of an azimuthally polarized beam and optical vortices in the tight focus cannot generate longitudinal electric components, which could tackle the generation of pure longitudinal magnetization. For an azimuthally polarized vortex beam with a topological charge of m, $\mathbf{E}^{Azi} = 1/2 e^{-i\pi/2}[\mathbf{E}^{\text{LHC}}(m-1) - \mathbf{E}^{\text{RHC}}(m+1)]$, the resultant light-induced magnetization can be expressed as

$$\mathbf{M}^{Azi}(\rho_s, \varphi_s, z_s) = \begin{bmatrix} \mathbf{M}_\rho \\ \mathbf{M}_\varphi \\ \mathbf{M}_z \end{bmatrix} = C' \begin{bmatrix} 0 \\ 0 \\ -\text{Re}[A_1(m) * A_2^*(m)] \end{bmatrix}. \tag{7}$$

When $m = 0$, no magnetization can be generated by focusing an azimuthally polarized beam. Interestingly, when $m = 1$ (or -1), the mutual effect between the polarization singularity of an azimuthally polarized beam and the optical vortex can lead to a Gaussian-shape-like pure longitudinal magnetization throughout the entire focal plane (Fig. 3). In addition, the orientation of the longitudinal magnetization, or the logical bit in AOMR, can be easily reversed by switching the helicity of the optical vortices. The axial cross section of the amplitude of the magnetization is shown in Fig. 3(b) with a dashed line. The longitudinal direction remains unchanged before and after the focal plane and the longitudinality is constantly one.
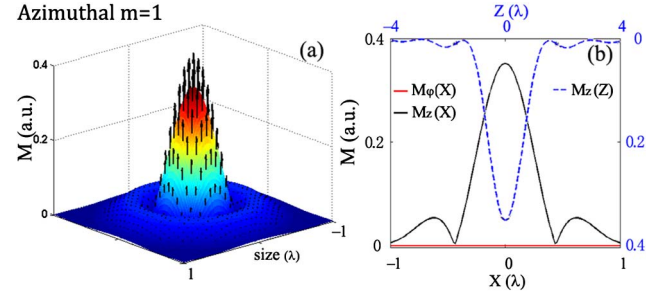

Fig. 3.   (a) Distribution of magnetization induced by the IFE by tightly focusing an azimuthally polarized beam with a topological charge $m = 1$. (b) Cross-section plots along the x axis (shown in the black solid line) and the z axis (shown in the blue dashed line). The azimuthal magnetization (M_φ) is zero in the focal vicinity.

Moreover, the generated magnetization field can be confined to a sub-diffraction-limited region. Further calculation indicates the lateral FWHM of the magnetization spot induced by tightly focusing azimuthally polarized vortex beams is only 84.9% compared with that of circularly polarized beams when NA = 0.95, valuing 0.5080λ and 0.5989λ, respectively, as shown in Fig. 4(a). This is depicted more clearly in the plot of the lateral FWHM as a function of the NA of the objective, as shown in Fig. 4(b). The enriched focal electric field components can lead to a large portion of transverse magnetic field components for a LHC polarized beam (23%) and for a radially polarized vortex beam (30%) at the NA of 0.95. On the contrary, the ratio of the longitudinal component to the total magnetization (M_z/M) by focusing an azimuthally polarized vortex beam is independent of the NA of the objective, owing to the nature of pure longitudinal magnetization [Fig. 4(c)].

In conclusion, we have theoretically investigated the light-induced magnetization by the IFE through focusing cylindrically polarized vortex beams with a high NA objective. It is found that the mutual effect between the optical vortices and the input polarization plays a critical role in determining the distribution and orientation of the focal magnetization. A pure longitudinal
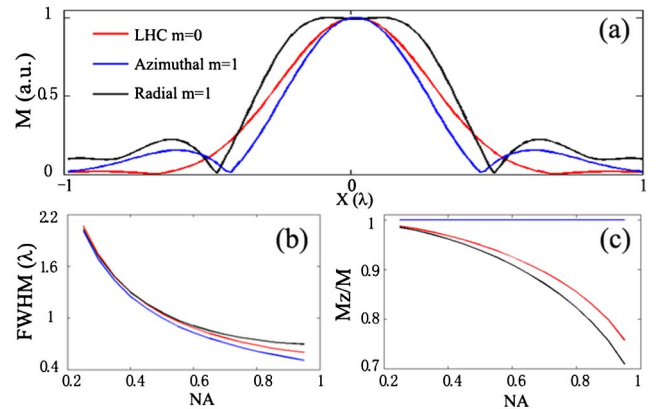

Fig. 4.   (a) Cross-section plots of the normalized magnetization for LHC polarized (red curve), radially polarized (black curve), and azimuthally polarized (blue curve) beams when NA = 0.95. (b) The lateral FWHMs of the magnetic field and (c) ratios of the longitudinal magnetic component (M_z/M), as a function of the NA of the objective.

magnetization distribution throughout the focal plane with a 15% reduced lateral FWHM can be generated by tightly focusing an azimuthally polarized vortex beam. This feature holds great potential in ultra-high density [16] AOMR. It may open a new avenue for controlling light–mater interaction in magnetic materials as well as for developing novel optomagnetic devices.

References

1. M. N. Baibich, J. M. Broto, A. Fert, F. N. Van Dau, F. Petroff, P. Eitenne, G. Creuzet, A. Friederich, and J. Chazelas, Phys. Rev. Lett. **61**, 2472 (1988).
2. L. P. Pitaevskii, Sov. Phys. JETP-USSR **12**, 1008 (1961).
3. A. V. Kimel, A. Kirilyuk, P. A. Usachev, R. V. Pisarev, A. M. Balbashov, and T. Rasing, Nature **435**, 655 (2005).
4. C. D. Stanciu, F. Hansteen, A. V. Kimel, A. Kirilyuk, A. Tsukamoto, A. Itoh, and T. Rasing, Phys. Rev. Lett. **99**, 047601 (2007).
5. S. Ali, J. R. Davies, and J. T. Mendonca, Phys. Rev. Lett. **105**, 035001 (2010).
6. M. Gu, *Advanced Optical Imaging Theory* (Springer, 2000).
7. X. Li, T. H. Lan, C. H. Tien, and M. Gu, Nat. Commun. **3**, 998 (2012).
8. L. E. Helseth, Opt. Lett. **36**, 987 (2011).
9. J. J. Yu, C. H. Zhou, and W. Jia, Opt. Commun. **283**, 4171 (2010).
10. V. Ravi, P. Suresh, K. B. Rajesh, Z. Jaroszewicz, P. M. Anbarasan, and T. V. S. Pillai, J. Opt. **14**, 55704 (2012).
11. Y. J. Zhang, Y. Okuno, and X. Xu, J. Opt. Soc. Am. B **26**, 1379 (2009).
12. Q. Zhan, Opt. Lett. **31**, 867 (2006).
13. D. Ganic, X. Gan, and M. Gu, Opt. Express **11**, 2747 (2003).
14. P. S. Pershan, J. P. van der Ziel, and L. D. Malmstrom, Phys. Rev. **143**, 574 (1966).
15. Y. J. Zhang, Y. Okuno, and X. Xu, Optik **121**, 2062 (2010).
16. Z. Gan, Y. Cao, R. A. Evans, and M. Gu, Nat. Commun. **4**, 2061 (2013).